8th INTERNATIONAL WORKSHOP ON ON-BOARD PAYLOAD DATA COMPRESSION (OBPDC 2022)

28-30 SEPTEMBER 2022

TOWARDS REAL-TIME MANAGEMENT OF SATELLITE MICROVIBRATIONS FOR ON-BOARD HYPERSPECTRAL IMAGE QUALITY ENHANCEMENT

Carlos Urbina Ortega[(1)(2)(3)], Eduardo Quevedo Gutiérrez[(2)], Laura Quintana[(2)], Samuel Ortega[(2)(4)], Lucana Santos Falcón[(1)(2)], Gustavo Marrero Callicó[(2)]

*[(1)]**European Space Research and Technology Centre (ESTEC)***
Keplerlaan 1, 2201AZ Noordwijk (ZH), NL
Email:carlos.urbina.ortega@ext.esa.int

*[(2)]**Research Institute for Applied Microelectronics (IUMA)***
University of Las Palmas de Gran Canaria (ULPGC), 35017 Gran Canaria, ES

*[(3)]**Telespazio Belgium Srl.***
Huygensstraat 34, 2201DK Noordwijk (ZH), NL

*[(4)]**Nofima - Norwegian Institute of Food Fisheries and Aquaculture Research***
Tromsø, NO

INTRODUCTION

The nature of earth observation satellites attitude and orbit control systems make them inherently susceptible to microvibrations (MVB) [1]. The largest sources of MVB in the current satellite platforms market are: reaction wheels, mechanical movements inside the thermal control subsystem, the changing thermal environment, and the vibration of the satellite structure due to its flexibility [2]. MVBs can be categorized according to its frequency into two classes: low-frequency and high-frequency. The first group affects the positioning accuracy of the image capture system, while the second one decreases the image spatial resolution. This work addresses the second group.

The spatial resolution of satellite on-board imaging systems has continuously increased in the last few years [3]. This has positioned MVBs as an important factor in the payload performance budget. This aspect becomes many times a driving limiting factor in the on-space spatial resolution of the earth-observation payloads [4]. Consequently, it is generally complicated to test and calibrate on-ground, due to the difficulties of simulating the real environment at integrated satellite-level. It also presents more variance on satellite platforms on which the quality control processes are less stringent (like NewSpace [5]).

This work proposes a lightweight multi-image super-resolution (MISR) algorithm that can help coping with MVB effects on hyperspectral (HS) payloads, resulting in an enhanced spatial and spectral image quality for the same on-board sensor and optics. The proposed algorithm addresses the following steps on the on-board image acquisition and image processing:

1. Sampling frequency of the image sensor.
2. Sub-pixel motion estimation between acquisitions: the current implementation works with MVB shifts of a resolution of a quarter of a pixel, but it can be generalized for smaller vibrations, and compensated with larger processing capability on-board.
3. Image super-resolution (SR) technique: once the oversampled images have been analyzed, the algorithm proposes an efficient technique to build images with ×2 and ×4 spatial resolution.
4. The influence of the HS sensor technology and optics in the super-resolution process.

The used metrics for comparison of spatial image quality results are based on Structural Similarity Index (SSIM) [6] and Peak Signal-to-Noise Ratio (PSNR), while the fundamental metric to assess the degradation of the spectral content is based on the Spectral Angle Mapper (SAM) [7]. The simulated results on satellite images are in the range of 400 nm to 2500 nm bands.

The proposed algorithm paves the way to a real-time processing system that could autonomously cope on-board with the satellite MVBs, avoiding the need for downloading extra images with the sole purpose of dealing with this problem on-ground. Furthermore, the algorithm could be used as well to obtain higher resolution images from the same sensor and optics on board, making more efficient use of the sensor capabilities. In both cases, it presents an alternative way to deal with the space-to-ground data bottleneck, which is general problem in earth-observation payloads.

MATERIALS AND METHODS

In the general MISR reconstruction case, three major steps can be identified:

1. Acquisition: capturing a sequence of images from the same scene with sub-pixel shifts between each of the images of the sequence.
2. Motion estimation: estimating the sub-pixel shift between the image taken as a reference for reconstruction and the rest of the sequence.
3. Restoration or super-resolution: reconstructing the HR image.

Each step will be treated separately in this section, together with the assumptions taken for data pre-processing between the acquisition from the sensor and algorithm input data. The metrics used to evaluate the results will also be explained at the end of the section.

HS data acquisition and preprocessing assumptions

Two different kinds of HS sensors are relevant to new space applications: push-broom and push-frame cameras. In both cases, the sampling frequency of earth-observation satellite imagers is commonly adjusted to offer the same spatial resolution *alongtrack* (defined by the integration time), and *acrosstrack* (defined by the pixel width) direction of the orbit motion. This is often an order of magnitude under the sensor sampling frequency capabilities. The proposed algorithm starts from the assumption that the sensor under study can indeed oversample the image sensor beyond the usual figures (the frequency of the pixel-width projection on Earth for squared pixel shape). This algorithm is only immediately applicable to push-frame sensors, although the technique is scalable to push-broom sensors with some adjustments (further details are included in DISCUSSION section).

Push-frame HS sensor assumptions

- The sensor is able to sample at least at double the frequency of the MVB that is needed to be addressed.
- Lens distortion is small or the on-board image pre-processing can compensate it.
- The illumination differences between exposures taken sequentially is negligible.
- The on-board data-handling system is able to cope with extra sensor data.
- MVB-induced motion can be simplified as global motion in a consecutive frate-to-frame basis.

HS data sequence generation

The image sequences used for this study have been artificially generated by applying a deterministic procedure to actual remote sensing images available in public repositories. The procedure to transform a single image into the necessary low-resolution sequence and high-resolution reference image is the following:

1. Define a rectangular crop of 128×512 pixels of the original image, leaving at least 16 pixels margin with respect to the end of the image on each side. All spectral information is kept in each pixel. This is called *reference frame*.
2. Apply a MVB function (Figure 1) making rectangular crops of the same size but centered at a different pixel. Their relationship to the reference frame is the motion vector defined in the MVB function. These images constitute the *high-resolution sequence* (HR sequence).
3. Decimate the images of the HR sequence by 2 and by 4 in X and Y dimensions, obtaining *low-resolution* (LR) and *very low-resolution* (VLR) frames respectively.
4. Compose a sequence of all the images that belong to the same decimation factor ×2 into a *low-resolution sequence*, and another sequence for the ones belonging to decimation factor ×4 into the *very low-resolution sequence*.

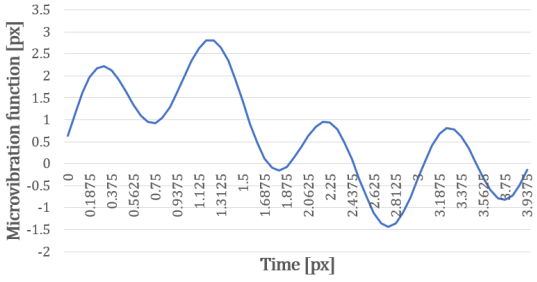

Figure 1. MVB function with a periodic and an aperiodic component.

Motion estimation

With the purpose of targeting near-real-time execution, the algorithm used for motion estimation is chosen to be one of the simplest ones: sum of absolute differences (SAD). It has been demonstrated to provide stable outcomes for pixel, half-pixel and quarter-pixel motion estimation when there is global motion. It works as follows:

1. Two images of the sequence under study, *reference* and *target*, are selected and interpolated to four times their size in X and Y dimension.
2. A search area is defined by the user (this is an optimization parameter). And then, a crop of the target image plus the search area is created, centered within the image.
3. The crop estimates its global motion vector against the reference image, calculating the SAD against all the possible positions within the search area.
4. The position with the minimum SAD is selected as the estimated motion vector.

As the images had been interpolated ×4, each unit in the vectors represent a quarter of a pixel with respect to the low-resolution reference images (e.g. resulting motion vector from SAD of [5,3] means [1.25, 0.75] in the reference image.

Image reconstruction

The approach used for SR in this study is the construction of HR HS images through the combination of several LR HS images with spectral information in the same bands, and sub-pixel displacement among them, which we denote as *frames*. Several frames compose what we denote as *sequence*. This follows the same rationale that denotes the baseline sensor as *push-frame*.

The algorithm is based on the concept that each LR frame can be considered a down-sampled version of a HR image, which will ultimately be used as the true scene [8]. The SR algorithm will align LR observations of the same sequence with sub-pixel accuracy for finally combining them into an HR grid. The correct and fast motion estimation is the cornerstone of this approach, and the application of a motion vector to individually to each of the bands in the HS image. The algorithm works as shown in Figure 2.

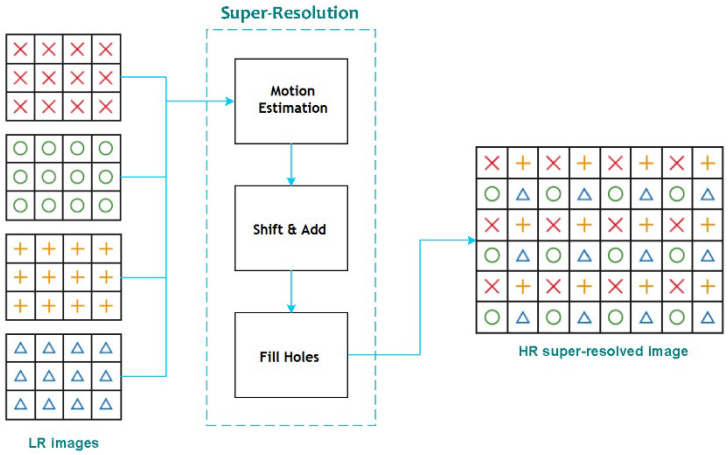

Figure 2. Diagram that synthesizes the super-resolution process in the developed algorithm.

Once the motion estimator has computed the set of motion vectors for each macroblock (MB) of the sequence, those vectors will be used to shift every MB in a higher resolution grid. The algorithm considers several parameters of the motion estimation and the surrounding pixels to weight the importance in the grid of each sub-pixel coming from different frames. It calculates a final value for the sub-pixel position using relatively simple mathematical function. This process has been denoted as *Shift and Add*. Finally, if there is any pixel which has been not filled throughout this process, it will be marked as a *hole*, and then interpolated using a bilinear surface interpolator. The same strategy will be applied to each band.

Evaluation metrics

To analyze the quality of the SR HS images obtained by the algorithms, three different metrics have been considered:

Structural Similarity Index (SSIM)

It measures the image degradation as perceived change in structural information, and it is calculated as follows [6]:

$$SSIM(x,y) = \frac{(2\mu_x\mu_y+C_1)+(2\sigma_{xy}+C_2)}{(\mu_x^2+\mu_y^2+C_1)\cdot(\sigma_x^2+\sigma_y^2+C_2)}, \quad (1)$$

where μ_x is the average of x, μ_y is the average of y, σ_x is the variance of x, σ_y is the variance of y, σ_{xy} is the covariance between x and y, $C_1 = (k_1 \cdot L)^2$ and $C_2 = (k_2 \cdot L)^2$are two constants to stabilise the division with weak denominator, $k_1 = 0.01$, $k_2 = 0.03$, and L is the dynamic range of the pixel values. Higher values mean better image quality, and 1 is the maximum value, meaning that reference and study image are structurally identical.

Peak Signal-to-Noise Ratio (PSNR)

It measures the relationship between the maximum possible power of a signal and the power of corrupting noise that affects the fidelity of its representation. It is an absolute error metric, and it is calculated as follows:

$$PSNR(x,y) = 10 \cdot log_{10}\left(\frac{R^2}{MSE(x,y)}\right), \quad (2)$$

where R is the maximum fluctuation in the input image data type, and MSE is the Minimum Square Error. It is important to understand that higher values mean better image quality.

Spectral Angle Mapper (SAM)

It measures the spectral degradation of a pixel with respect to a reference spectral signature, in the form of an angle between their two vector representations. For evaluating image quality, the average value across the entire image is considered. It is a full-reference metric and it is calculated as follows [7]:

$$SAM(a_n, \hat{a}_n) = arccos\left(\frac{\langle a_n, \hat{a}_n \rangle}{\|a_n\| \cdot \|\hat{a}_n\|}\right), \quad (3)$$

where a_n and $\hat{a}_n$ are the corresponding individual pixel spectral vectors of the reference and super-resolved HSI respectively. Closer to zero values mean better image quality, and 0 degrees means identical spectral signature between reference and study image.

Scoring methodology

Two different scores are proposed. Their purpose is a more direct understanding of the performance of the proposed SR algorithm with respect to other methods found in the literature.

$$Score = \frac{PSNR \cdot SSIM}{SAM}, \quad (4)$$

where PSNR and SAM are defined in equations (1), (2) and (3).
Examining equation (4), the following properties are noted:

- The highest the score, the better the algorithm.
- Metrics that have *infinity* (∞) as ideal value are in direct proportion with the score.
- Metrics that have *zero* (0) as ideal value are in inverse proportion with the score.

Processing platform

All the results presented in this publication have been processed in a commercial computer with a CPU Intel® Core™ i7-3540M running at 3.0 GHz and 8 Gigabytes of DDR3 RAM clocked at 1600 MHz. The MATLAB® version used for image visualization is 2020a, and the algorithm is implemented in C language.

RESULTS

A set of three HS sequences are presented to analyze the performance of the algorithm. As a starting point, the popular public HS image of Pavia University [9] is used. Furthermore, results about this image aid generalizing the relevance of the algorithm to different sensors and data applications. Such analysis is presented in [10].
The other two images are artificial sequences created using the procedure in section *HS data sequence generation* from two original images of Hyperion payload of the USGS EO-1 satellite available in the database [11]. These images are in the range from the Visible Human Spectrum to the SWIR (Short-Wave Infrared, from 400-2500 nm). The escalation factor (EF) denotes the spatial resolution enhancing objective of the algorithm; results for ×2 and ×4 have been obtained in all the image sequences. N denotes the number of frames that have been combined within the sequence under study.

La Reunion

This image is an extract from a real remote sensing measurement labelled as EO1H1530752015280110KF (Hyperion payload of the USGS EO-1 satellite [11]). The results are presented in Figure 5 for visual inspection, and in Figure 6 for quantitative assessment. Using EF=2 it can be appreciated that the sharpness of the different elements in the image has improved, in particular the diagonal lines and small objects, and the contrast has increased. Furthermore, using EF=4 it is more evident that the interpolated image has difficulties to follow diagonal straight lines, producing clear squared defects, while in the super-resolved image the overall contrast has diminished.

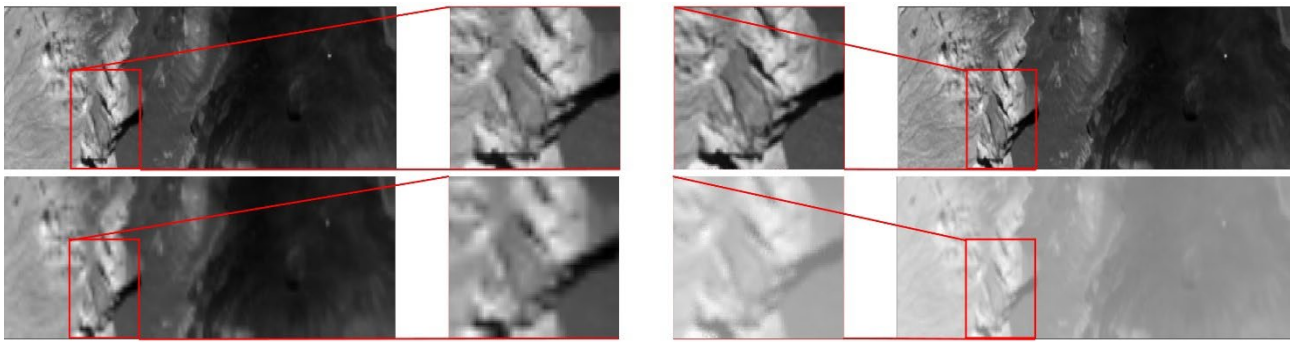

Figure 3. Visual inspection for image *La Reunion*: *top*, EF = 2, and *bottom*, EF = 4 at band corresponding to 1029 nm wavelength. On the *left*, the interpolated images, and its corresponding zoom over a representative area; on the *right*, the super-resolved images with a zoom in the exact same area for easier visual comparison.

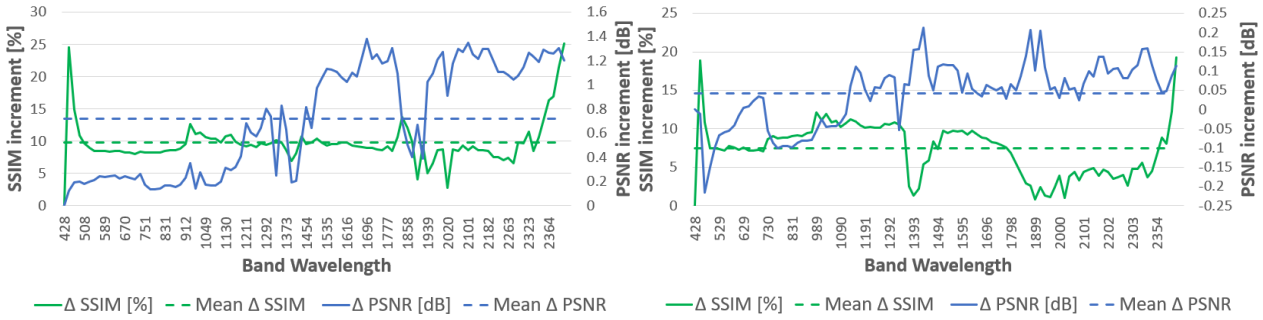

Figure 4. Variation of the performance of the proposed SR algorithm across the spectrum for PSNR and SSIM metrics in sequence *La Reunion*: *left* EF=2, and *right* EF=4. Average values for both performances along the studied spectra are presented in dashed lines as a general indication.

In quantitative terms, the SSIM improvement curve is quite uniform along the whole spectrum for EF=2, while very irregular for the EF=4. The PSNR improvement is significant in EF=2, although only in the second half of the spectrum, and it is very mild overall in the EF=4 case.

Additionally, the average SAM over the image has been calculated for both images with respect to the reference image, with an average improvement of 13.03% for the ×2, and 1.65% for ×4. An example of the gain obtained in an individual pixel with regards to the spectral signature is presented in Figure 7.

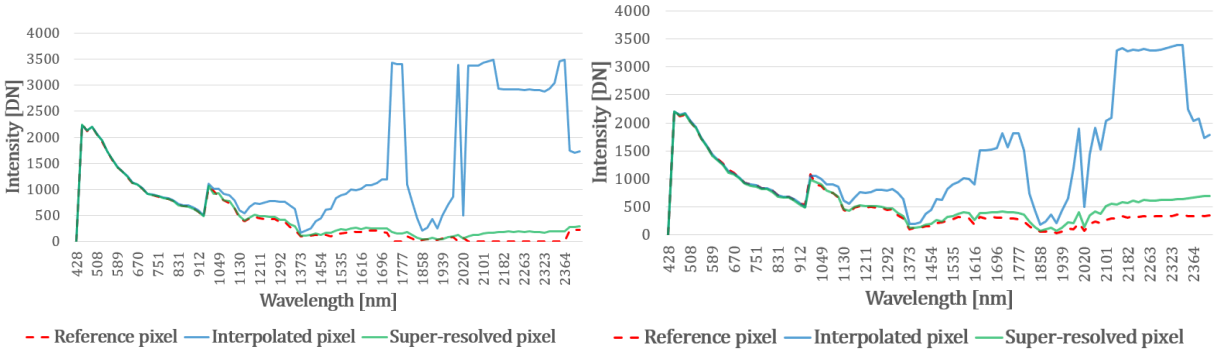

Figure 5. Spectral signature for pixels of *La Reunion*: *left*, pixel (28,438) of ×2, and *right*, pixel (21,447) of ×4 image.

Guraidhoo (Maldives)

This image is as well an extract from a real remote sensing measurement labelled as EO1H1450572005025110KX from the Hyperion payload of the USGS EO-1 satellite [11]. The results are presented in Figure 8 for visual inspection, and in Figure 9 for quantitative assessment.

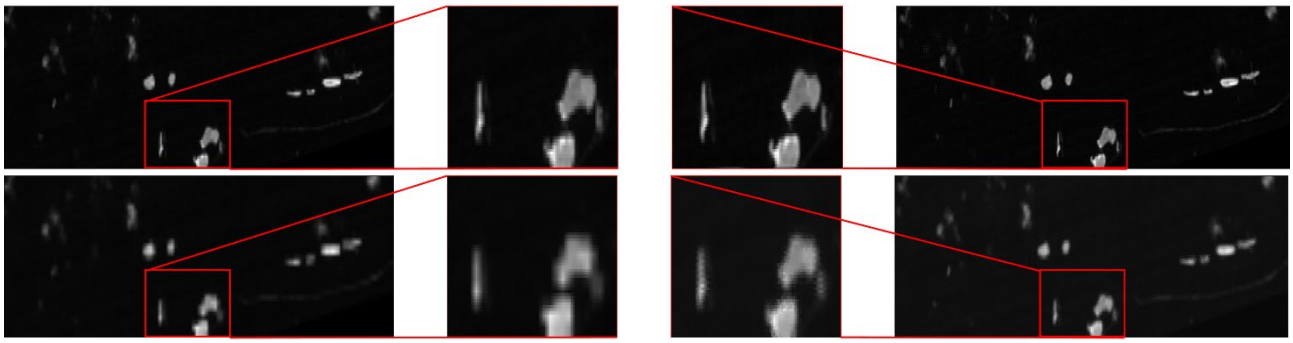

Figure 6. Visual inspection for image *Guraidhoo*: *top*, EF = 2, and *bottom*, EF = 4 at band corresponding to 790 nm wavelength. On the *left*, the interpolated images and its corresponding zoom over a representative area; on the *right*, the super-resolved images with a zoom in the exact same area for easier visual comparison.

Using EF = 2, it can be appreciated that the sharpness of the different elements in the image has improved, in particular the diagonal lines and small objects (smaller islands and bays). Using EF = 4 it is more evident that the interpolated image has difficulties to follow small details and objects, producing clear squared defects, while in the super-resolved image some artifacts appear in the tiniest details (which has been demonstrated to depend on the selected images within the super-resolution sequence).

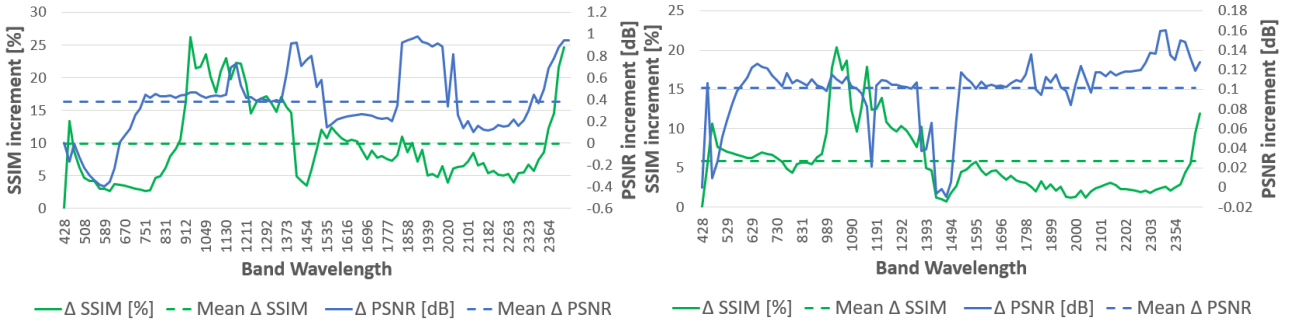

Figure 7. Variation of the performance of the proposed SR algorithm across the spectrum for PSNR and SSIM metrics in sequence *Guraidhoo*: *left* EF=2, and *right* EF=4. Average values for both performances along the studied spectra are presented in dashed lines as a general indication.

Quantitaively, the SSIM improvement curve is irregular along the spectrum for EF=2 and EF=4, nevertheless presenting a significant better performance than average in the range 900-1300 nm wavelength. The PSNR improvement is mild overall in both EF=2 and EF=4 cases.

Similarly to *La Reunion*, the average SAM over the image has been calculated, with an average improvement of 12.18% for the ×2, and 6.27% for ×4. An example of the gain obtained in an individual pixel with regards to the spectral signature is presented in Figure 10.

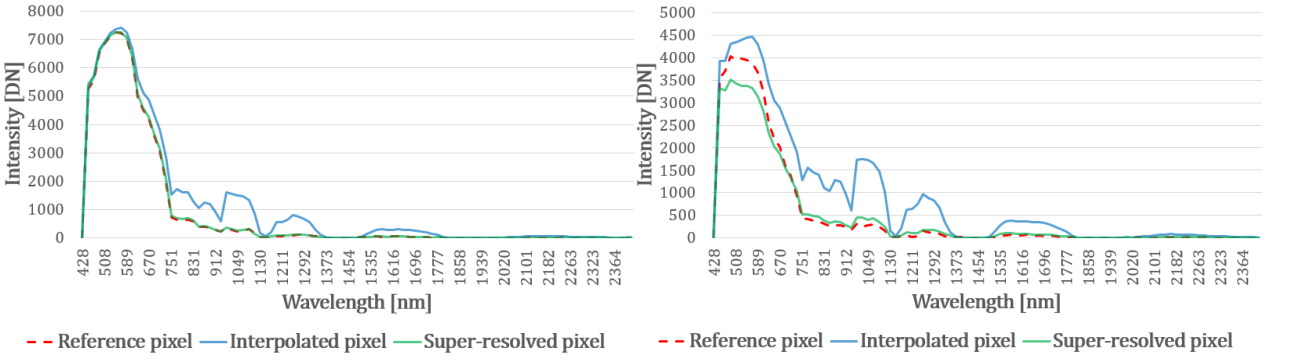

Figure 8. Spectral signature for pixels of *La Reunion*: *left*, pixel (72,386) of ×2, and *right*, pixel (55,423) of ×4 image.

DISCUSSION

To summarize the overall performance of the algorithm, a scoring system has been proposed in equation (4). Its comparison with the bilinear interpolation following such score is presented in Table 1. As deeply analyzed in [10] and here demonstrated valid also in remote sensing images in the SWIR range, despite its simplicity, the algorithm can be competitive against some state-of-the-art techniques.

Table 1. Comparison of the performance of the proposed SR algorithm against a bilinear interpolation following the scoring system presented in equation (4).

Score\Sequence	La Reunion ×2	La Reunion ×4	Guraidhoo ×2	Guraidhoo ×2	Runtime (s)
Bilinear Interpolation	831.82	242.79	1338.59	449.11	0.072
Proposed SR algorithm	1069.02	264.16	1672.73	501.91	1.67

The execution time obtained in a commercial computer without hardware optimization leads to the conclusion that a real-time execution at-the-edge is feasible in space application. In such a case, there would be a number of MVB cases that could be dealt with autonomously by the payload. Furthermore, better resolution images with the same sensor could even be obtained directly on-board thanks to some of MVB scenarios, not needing to download multiple images of the same scene to ground for post-processing. This represents an important latency and data volume reduction case. It should be kept in mind that the capability for dealing with MVB is bounded by the relation between the frequency of the MVB itself, and the sampling frequency of the sensor.

Even if it is clear that there is a strong dependency on the selected images regarding the performance of the algorithm for the different analyzed bands, the results on ×2 scalation seem to be stable around 10% extra gain on average with respect to a linear interpolation when SSIM is discussed, while PSNR response is not conclusive.

The potential to improve the overall spectral signature can be well appreciated in both the results of *La Reunion* and *Guraidhoo* sequences. In particular, it is remarkable the capability to follow the spectral firm of pixels in areas that define the borders of different materials, as the one reported in Figure 7 and Figure 10. This can be particularly useful for later semantic segmentation and environmental control applications (wildfire detection, disaster assessment, oil spill, to mention some).

Part of the study has developed a similar technique for push-broom HS imagers, although the results where less conclusive, and too dependent on the decimation model, which emulates the specific sensor and optics. Further development on that line is one of the future lines of research as well as the embedded implementation in a rad-hard processor or FPGA to demonstrate the real-time capabilities.

CONCLUSIONS

In conclusion, a proposal for real-time algorithm that deals with MVB in push-frame hyperspectral sensors on board satellites has been presented, and its performance was demonstrated and compared with other algorithms. Its capability to improve the SSIM and SAM for bands in 400-2500 nm wavelengths in remote sensing HS images is remarkable and it can be particularly interesting for semantic segmentation at-the-edge and for small satellites with limited MVB control.

REFERENCES

[1] C. Dennehy and O.S. Alvarez-Salazar, “Spacecraft Micro-Vibration: A Survey of Problems, Experiences, Potential Solutions, and Some Lessons Learned”, NASA/TM−2018-220075.

[2] Tang, Xinming, Junfeng Xie, Hong Zhu, and Fan Mo. 2020. "Overview of Earth Observation Satellite Platform Microvibration Detection Methods" Sensors 20, no. 3: 736. https://doi.org/10.3390/s20030736.

[3] P. Ghamisi et al., "Advances in Hyperspectral Image and Signal Processing: A Comprehensive Overview of the State of the Art," in IEEE Geoscience and Remote Sensing Magazine, vol. 5, no. 4, pp. 37-78, Dec. 2017, doi: 10.1109/MGRS.2017.2762087

[4] Marcello Remedia and Guglielmo S Aglietti, “Modelling Micro-Vibrations Transmission in Spacecraft Structure”, IAC Proceedings of 2014.

[5] Blommaert, Joris & Delauré, B. & Livens, Stefan & Nuyts, Dirk & Moreau, Vincent & Callut, Eric & Habay, Gerard & Vanhoof, Koen & Caubo, Michel & Vandenbussche, Jan & Deep, Atul & Minoglou, Kyriaki. (2017). “CHIEM: A new compact camera for hyperspectral imaging”.

[6] Wang, Z., Bovik, A., Sheikh, H., Simoncelli, E., 2004. “Image quality assessment: From error visibility to structural similarity”. Image Processing, IEEE Transactions on 13, 600 – 612. doi:10.1109/TIP.2003.819861

[7] Yuhas, R.H., Goetz, A.F.H., Boardman, J.W., 1992. “Discrimination among semi-arid landscape endmembers using the spectral angle mapper (SAM) algorithm”, in: NASA AVIRIS Workshop 92, pp. 147 – 149.

[8] Quevedo Gutiérrez, E., Sánchez, L., Marrero Callico, G., Tobajas, F., Cruz, J., Sosa, V., Sarmiento, R., 2018. “Super-resolution with selective filter based on adaptive window and variable macro-block size”. Journal of Real-Time Image Processing 15, 389–406. doi:10.1007/s11554-015-0489-3.

[9] Dell’Acqua, F., Gamba, P., Ferrari, A., Palmason, J., Benediktsson, J., Arnason, K., 2004. “Exploiting spectral and spatial information in hyperspectral urban data with high resolution”. IEEE Geoscience and Remote Sensing Letters 1, 322–326. doi:10.1109/LGRS.2004.837009.

[10] Carlos Urbina Ortega et al., “Towards real-time hyperspectral multi-image super-resolution reconstruction applied to histological samples”, Unpublished

[11] USGS EROS Archive for EO-1 Hyperion data. https://www.usgs.gov/centers/eros/science/usgs-eros-archive-earth-observing-one-eo-1-hyperion